



Flame brush characteristics and burning velocities of premixed turbulent methane/air Bunsen flames



Parsa Tamadonfar*, Ömer L. Gülder

Institute for Aerospace Studies, University of Toronto, 4925 Dufferin Street, Toronto, Ontario M3H 5T6, Canada

ARTICLE INFO

Article history:

Received 10 January 2014

Received in revised form 27 March 2014

Accepted 19 June 2014

Available online 9 August 2014

Keywords:

Premixed turbulent flames

Flame brush thickness

Turbulent burning velocity

ABSTRACT

The flame brush characteristics and turbulent burning velocities of premixed turbulent methane/air flames stabilized on a Bunsen-type burner were studied. Particle image velocimetry and Rayleigh scattering techniques were used to measure the instantaneous velocity and temperature fields, respectively. Experiments were performed at various equivalence ratios and bulk flow velocities from 0.7 to 1.0, and 7.7 to 17.0 m/s, respectively. The total turbulence intensity and turbulent integral length scale were controlled by the perforated plate mounted at different positions upstream of the burner exit. The normalized characteristic flame height and centerline flame brush thickness decreased with increasing equivalence ratio, total turbulence intensity, and longitudinal integral length scale, whereas they increased with increasing bulk flow velocity. The normalized horizontal flame brush thickness increased with increasing axial distance from the burner exit and increasing equivalence ratio. The non-dimensional leading edge and half-burning surface turbulent burning velocities increased with increasing non-dimensional turbulence intensity, and they decreased with increasing non-dimensional bulk flow velocity when other turbulence statistics were kept constant. Results show that the non-dimensional leading edge and half-burning surface turbulent burning velocities increased with increasing non-dimensional longitudinal integral length scale. Two correlations to represent the leading edge and half-burning surface turbulent burning velocities were presented as a function of the equivalence ratio, non-dimensional turbulence intensity, non-dimensional bulk flow velocity, and non-dimensional longitudinal integral length scale. Results show that the half-burning surface turbulent burning velocity normalized by the bulk flow velocity decreased as the normalized characteristic flame height increased.

© 2014 The Combustion Institute. Published by Elsevier Inc. All rights reserved.

1. Introduction

Premixed turbulent combustion is being studied widely because of its importance in the development of low-emission combustion devices such as engines for transportation, and lean-burn gas turbines for power generation [1]. Despite the ongoing advance in understanding the premixed turbulent combustion mechanism, there still exist many unresolved problems regarding the fundamental properties of such flames. The knowledge of flame brush characteristics and turbulent burning velocity are essential for the design of premixed combustion devices and numerical model testing [2]. The premixed turbulent flame geometries are mainly divided into the “Envelope” category (Bunsen-type flames), “Oblique” category (rod-stabilized V-shaped flames), “Unattached”

category (counterflow and low-swirl flat flames), and spherical expanding flames [3–5].

In this study, the experiments were performed on a Bunsen-type burner. The characteristics of the flame brush are classified into two parts: (1) the flame height, $H_{(c)}$, and (2) the flame brush thickness, δ_T . The quantitative value of flame height changes significantly by selecting different values of mean progress variable, (c) , whereas the observed trend of flame height remains unchanged with different flame/flow properties at a constant mean progress variable [6]. Previous results show that the flame height decreases with increasing the equivalence ratio from ultra-lean to stoichiometric mixtures [6–9]. It is observed that the flame height decreases with increasing total turbulence intensity, u' , at a constant bulk flow velocity, U_B , see, e.g., [8]. Moreover, Griebel et al. [9] reported that the flame height is independent of pressure, while it decreases by preheating the reactants. They observed that the centerline flame brush thickness, $\delta_{T,0}$, decreases with increasing the equivalence ratio from ultra-lean to stoichiometric methane/air flames, and it increases with increasing total turbulence intensity. In

* Corresponding author.

E-mail addresses: tamadonfar@utias.utoronto.ca, parsa.tamadonfar@utoronto.ca (P. Tamadonfar).

addition, the growing behavior of the horizontal flame brush thickness, $\delta_{T,h}$, with increasing axial distance from the flame-holder for the Bunsen-type, V-shaped, and confined oblique flames was reviewed by Lipatnikov and Chomiak [2].

Several correlations are proposed in the literature to estimate the turbulent burning velocity, S_T , of premixed turbulent flames based on the turbulence statistics, namely the total turbulence intensity and turbulent length scale, see, e.g., [2,10,11]. Gülder [10] proposed conceptual models for the estimation of turbulent burning velocity for three combustion regimes. These models were tested by comparing them to the measured data of various experimental rigs covering the range from flames stabilized in ducts to expanding flames. Liu et al. [11] proposed a general correlation in order to predict the turbulent burning velocity of spherical expanding flames under various pressures and turbulent Reynolds numbers. All of their measurements lie on a single curve of the form $(S_{T,(c)=0.5} - S_L^0)/u' = 0.14Da^{0.47}$, where $S_{T,(c)=0.5}$, S_L^0 , and Da are the half-burning surface turbulent burning velocity, unstrained premixed laminar burning velocity, and turbulent Damköhler number, respectively. Lipatnikov and Chomiak [2] reviewed the influence of these statistics on the turbulent burning velocity using the data reported by various researchers. It is widely accepted that the turbulent burning velocity increases with the total turbulence intensity up to moderate turbulence levels, whereas it shows a decreasing tendency when the turbulence level becomes more intense. The latter is known as the “bending” phenomenon. The possibility of flamelets merging along with the gas expansion may be the reason behind the aforementioned mechanism [4]. As noted in [2], not many comprehensive studies have been performed on the influence of turbulent integral length scale on the turbulent burning velocity. However, most of the experimental data and empirical correlations show an increase of the turbulent burning velocity with increasing turbulent integral length scale. It should be mentioned that obtaining a universal correlation for the turbulent burning velocity has not been successful mostly due to a large scatter of the experimental data available in the literature [12]. It appears that using the turbulent burning velocity data from different flame geometries could be the culprit in unsuccessful attempts to have a universal correlation [5,12]. Therefore, it is suggested that the turbulent burning velocity data from one flame category should only be used for a geometry-specific correlation for the turbulent burning velocity in view of the fact that the flame front wrinkling and boundary conditions seems to be geometry-dependent [5].

In addition to the total turbulence intensity and turbulent length scale, Filatyev et al. [4] recommended to include further parameters such as the bulk flow velocity and burner width in the turbulent burning velocity correlation of Bunsen-type flames. They stated that increasing the bulk flow velocity and burner width elongate the flame height. This may result in an increase in the turbulent burning velocity due to an increase in flame surface wrinkling. This hypothesis is supported by the experimental data showing that the turbulent burning velocity increases with increasing bulk flow velocity, see, e.g., [4,13,14]. However, the observed trend may not be solely due to the effect of bulk flow velocity since the total turbulence intensity increases simultaneously with the bulk flow velocity in these experiments. To the best of the authors' knowledge, there has not been any systematic investigation conducted on the influence of bulk flow velocity on the turbulent burning velocity when other turbulence statistics and burner geometry are kept constant. Therefore, studying the effect of bulk flow velocity on the turbulent burning velocity of Bunsen-type flames may contribute to the explanation of the disparity among measurements available.

In the current study, the first objective was to determine the influences of equivalence ratio, total turbulence intensity, bulk

flow velocity, and longitudinal integral length scale on the flame brush characteristics of premixed turbulent Bunsen-type flames. The second objective was to investigate the effects of the aforementioned parameters on the turbulent burning velocity, and to incorporate these parameters in an empirical expression to represent the turbulent burning velocity of Bunsen-type flames.

2. Experimental methodology

2.1. Bunsen-type burner

An axisymmetric Bunsen-type burner with a nozzle inner diameter, D , of 11.1 mm was used to generate premixed turbulent conical flames. This burner has been previously used in this laboratory to study the structure of premixed turbulent flame fronts, see, e.g., [15], and the geometry of its components was documented in detail in [16]. The calibrated mass flow meters were used to control the flow rates of the filtered air and methane grade 2.0. The accuracy for each of the mass flow meter was $\pm 0.80\%$ on its reading, and $\pm 0.20\%$ on its full scale. The premixed turbulent flame was anchored to the rim of the burner using an annular premixed ethylene/air pilot flame. The turbulence was produced using two perforated plates, that is, PP-I and PP-II. The holes for each of the perforated plate are arranged in a hexagonal array. The geometrical properties of the perforated plate are characterized by the hole diameter (d), mesh size (M), and blockage ratio (β). Table 1 summarizes geometrical properties for perforated plates used in this study.

2.2. Flow field characterization and experimental conditions

The turbulence statistics in the flow field were characterized using the two-dimensional particle image velocimetry technique. A double-pulsed Nd:YAG laser was used as a light source in order to illuminate the seeding particles with a maximum energy and wavelength of 200 mJ/pulse and 532 nm, respectively. These particles were generated by atomizing olive oil to sub-micron droplets using a nebulizer. The laser sheet was formed by passing the laser beam through a LaVision light sheet optical assembly. This assembly consisted of two spherical lenses, $f = +85$ and -75 mm, and a cylindrical lens, $f = -20$ mm. The laser sheet had a full-width-at-half-maximum (FWHM) of approximately 300 μm at the burner centerline. The experimental images were captured using a LaVision Imager pro X camera with a resolution of 2048×2048 px². A Sigma macro lens with a focal length of 105 mm operating at $f/8$ was mounted on the camera, and a 532 nm bandpass filter was attached to the lens to decrease the intrusion of unsought wavelengths from the surrounding environment on the camera's CCD. The axial and radial velocity components were calculated using the DaVis 7.2 software (FlowMaster, LaVision). For each experimental condition, five hundred image pairs were acquired at a frequency of 6 Hz under the non-reacting condition. A multi-pass vector evaluation algorithm was applied on each image pair with interrogation box sizes decreasing from 64×64 to 32×32 px² with a 50% overlap. This resulted in a resolution and vector spacing of approximately 960 and 480 μm , respectively. The time delay between laser pulses was adjusted for each experimental condition in order to confirm that the displacement of

Table 1
Summary of geometrical properties for perforated plates.

Perforated plate	d (mm)	M (mm)	β (%)
PP-I	1.1	1.3	43
PP-II	0.9	1.3	62

seeding particles was less than a quarter of the final interrogation box size.

In this study, four sets of experiments were performed. Table 2 summarizes the upstream position(s) of the grid(s) from the burner exit, bulk flow velocity, total turbulence intensity, and longitudinal integral length scale under non-reacting conditions for all sets of experiments. The profiles of the mean axial velocity, $\langle U \rangle$, normalized by the bulk flow velocity, U_B , as a function of the normalized radial distance, r/D , for all sets of experiments at $h/D = 0.5$ are shown in Fig. 1, where r is the radial distance from the centerline of the burner, and h is the axial distance from the burner exit. The total volumetric flow rate was used to determine the bulk flow velocity for each set of experiments. The mean axial velocity profiles of experimental sets II and III resemble to an almost parabolic profile which could be attributed to the coalition of small turbulent jets generated by the holes of the perforated plate [17]. These profiles are more like top hat across the burner exit for sets I and IV where the perforated plates are mounted far from the burner exit. Experimental measurements of Chen and Bilger [17] showed a similar trend. The total turbulence intensity, u' , and longitudinal integral length scale, Λ_L , were controlled by the geometry and upstream position of the perforated plate from the burner exit. Due to the axisymmetric nature of the flow, the root-mean-square (r.m.s) of velocity fluctuations in the radial, $\langle v^2 \rangle^{1/2}$, and azimuthal, $\langle w^2 \rangle^{1/2}$, directions were assumed to be equal. Therefore, the r.m.s of velocity fluctuations in the radial, $\langle v^2 \rangle^{1/2}$, and axial, $\langle u^2 \rangle^{1/2}$, directions were used to estimate the total turbulence intensity from $u' = \sqrt{(2\langle v^2 \rangle + \langle u^2 \rangle)/3}$. The profiles of the axial, radial, and total velocity fluctuations are shown in Fig. 2(a–c), respectively. These profiles are uniform for $r/D < 0.3$, whereas they increase considerably near the rim of the burner. Similar observations were noted previously in [13,18]. The longitudinal integral length scale was estimated by integrating the longitudinal velocity correlation coefficient, $f(\Delta x)$, over the velocity vector spacing in the axial direction, Δx [19]. The longitudinal velocity correlation coefficient was obtained from $f(\Delta x) = \langle u(h)u(h + \Delta x) \rangle / \langle u(h)^2 \rangle$, where u is the velocity fluctuations in the axial direction. This integration was performed until the first location at which the longitudinal velocity correlation coefficient was equal to zero. The profile of the longitudinal velocity correlation coefficient for the first set of experiments at $h/D = 0.5$ is shown in Fig. 3. The uncertainty associated with estimation of the longitudinal integral length scale was approximately 25%. For all experimental conditions, these turbulence properties, that is, u' and Λ_L , were averaged in a region between

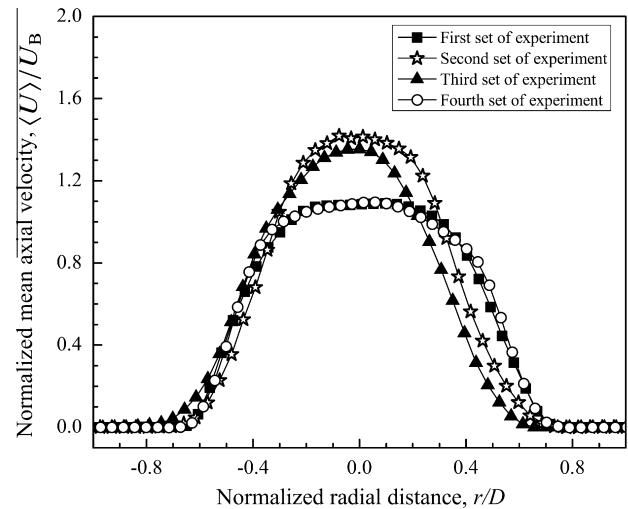


Fig. 1. Normalized mean axial velocity profiles as a function of the normalized radial distance for all sets of experiments at $h/D = 0.5$.

$-0.25 < r/D < 0.25$ and $0.1 < h/D < 0.5$. According to the results presented in Table 2, the total turbulence intensity increased by a factor of 3.5 from the first to the second set of experiments, whereas the bulk flow velocity and longitudinal integral length scale were kept constant. From the third to the fourth set of experiments, the bulk flow velocity increased from 7.7 to 17.0 m/s, whereas the total turbulence intensity and longitudinal integral length scale were kept constant. The bulk flow velocity and total turbulence intensity were kept constant for the first and fourth sets, whereas the longitudinal integral length scale increased from 1.5 to 2.2 mm. These sets of experiments permit an independent investigation of the total turbulence intensity, bulk flow velocity, and longitudinal integral length scale on the flame brush characteristics and turbulent burning velocity.

The summary of all flame conditions is tabulated in Table 2. The equivalence ratio, ϕ , was changed from 0.7 to 1.0 for each set of experiments. The unstrained premixed laminar burning velocity, S_L^0 , was estimated using the Cantera package [20] with the GRI-Mech 3.0 mechanism [21]. These numerical values were in good agreement with experimental measurements previously reported in [22–24]. The Zel'dovich thickness, δ_f , was determined by calculating the ratio of the reactant mass diffusivity to the unstrained

Table 2

Summary of experimental conditions. Symbols: h_e = upstream position of the grid from the burner exit; ϕ = equivalence ratio; U_B = bulk flow velocity; u' = total turbulence intensity; S_L^0 = unstrained premixed laminar burning velocity; Λ_L = longitudinal integral length scale; δ_f = Zel'dovich thickness; Re_{Λ_L} = turbulent Reynolds number; Ka = turbulent Karlovitz number; Da = turbulent Damköhler number.

Set of exp.	Flame	ϕ	U_B (m/s)	u' (m/s)	S_L^0 (m/s)	Λ_L (mm)	U_B/S_L^0	u'/S_L^0	Λ_L/δ_f	u'/U_B (%)	Re_{Λ_L}	Ka	Da
I Grid type: PP-I, PP-II h_e (mm): 11, 100	A1	0.7	17.0	0.69	0.198	1.5	85.6	3.5	13.5	4.1	65	2.9	3.9
	B1	0.8	17.0	0.69	0.279	1.5	60.9	2.5	19.0	4.1	65	1.5	7.7
	C1	0.9	17.0	0.69	0.345	1.5	49.3	2.0	23.5	4.1	65	0.9	11.7
	D1	1.0	17.0	0.69	0.386	1.5	44.0	1.8	26.4	4.1	65	0.7	14.8
II Grid type: PP-II h_e (mm): 11	A2	0.7	17.0	2.44	0.198	1.4	85.6	12.3	12.8	14.4	218	19.6	1.0
	B2	0.8	17.0	2.44	0.279	1.4	60.9	8.7	18.1	14.4	218	9.8	2.1
	C2	0.9	17.0	2.44	0.345	1.4	49.3	7.1	22.4	14.4	218	6.4	3.2
	D2	1.0	17.0	2.44	0.386	1.4	44.0	6.3	25.2	14.4	218	5.1	4.0
III Grid type: PP-II h_e (mm): 11	A3	0.7	7.7	0.74	0.198	2.2	38.9	3.7	19.9	9.5	103	2.6	5.4
	B3	0.8	7.7	0.74	0.279	2.2	27.6	2.6	28.1	9.5	103	1.3	10.6
	C3	0.9	7.7	0.74	0.345	2.2	22.3	2.1	34.8	9.5	103	0.9	16.3
	D3	1.0	7.7	0.74	0.386	2.2	19.9	1.9	39.1	9.5	103	0.7	20.5
IV Grid type: PP-I h_e (mm): 89	A4	0.7	17.0	0.74	0.198	2.2	85.6	3.7	21.0	4.4	103	2.6	5.6
	B4	0.8	17.0	0.74	0.279	2.2	60.9	2.7	28.5	4.4	103	1.3	10.7
	C4	0.9	17.0	0.74	0.345	2.2	49.3	2.2	34.1	4.4	103	0.9	15.9
	D4	1.0	17.0	0.74	0.386	2.2	44.0	2.0	40.2	4.4	103	0.7	20.1

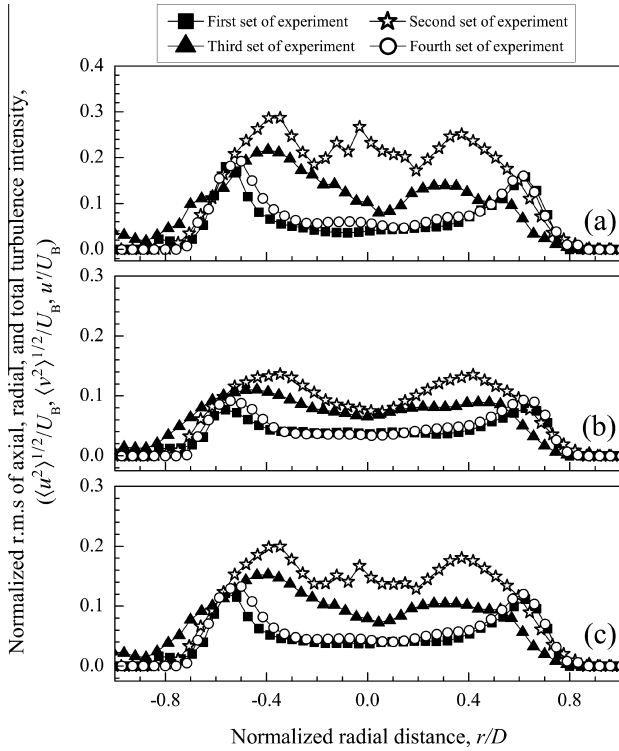


Fig. 2. Normalized r.m.s. of (a) axial, (b) radial, and (c) total velocity fluctuations for all sets of experiments at $h/D = 0.5$.

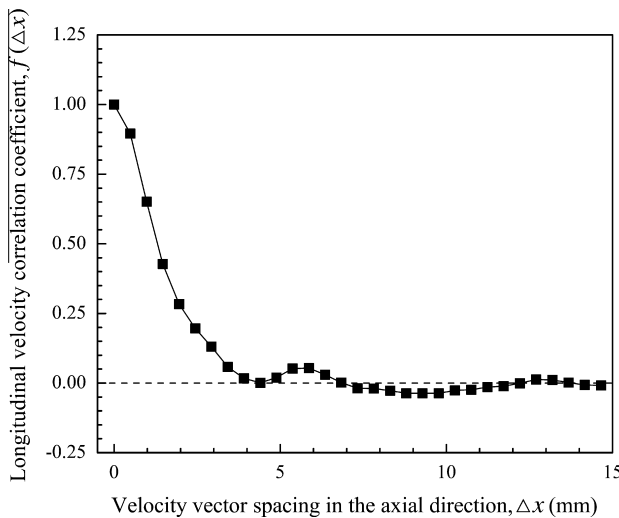


Fig. 3. Longitudinal velocity correlation coefficient as a function of the velocity vector spacing in the axial direction for the first set of experiments on the centerline of the burner at $h/D = 0.5$.

premixed laminar burning velocity [1]. The turbulent Reynolds, Karlovitz, and Damköhler numbers were evaluated from $Re_{\Lambda_L} = u' \Lambda_L / \nu$, $Ka = (\delta_f / \eta)^2$, and $Da = \Lambda_L S_L^0 / \delta_f u'$, respectively, where ν is the reactant kinematic viscosity, and η is the Kolmogorov length scale evaluated from $\eta = \Lambda_L Re_{\Lambda_L}^{-3/4}$.

The experimental conditions were plotted on a Borghi–Peters regime diagram for premixed turbulent combustion [25,26] as shown in Fig. 4. Peters [26] proposed that the corrugated flamelets regime separates from the thin reaction zones regime at $Ka = 1$, and the thin reaction zones from the broken reaction zones regime at $Ka = 100$ using the following expression:

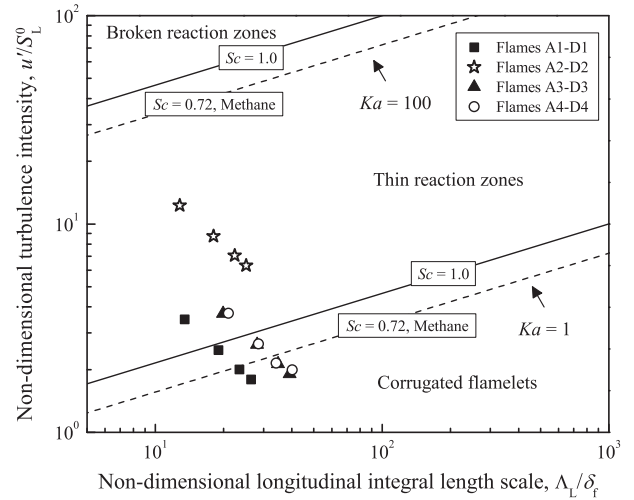


Fig. 4. Experimental conditions on a Borghi–Peters regime diagram for premixed turbulent combustion [25,26].

$$\frac{u'}{S_L} = Ka^{2/3} \left(\frac{\Lambda_L}{\delta_f} \right)^{1/3} \quad (1)$$

The above expression was developed for the mixture with a Schmidt number, Sc , equal to unity, where the Schmidt number is the ratio of the reactant kinematic viscosity to the mass diffusivity. It should be stated that the Schmidt number for methane/air mixtures is approximately 0.72. Therefore, the lines that separate the combustion regimes from each other are different from the lines proposed by Peters [26]. In order to obtain a new expression for non-unity Schmidt number, the same mathematical procedure as [26] was used with the exception that the kinematic viscosity and mass diffusivity were retained in the formulation. This results into the following expression:

$$\frac{u'}{S_L} = Ka^{2/3} Sc \left(\frac{\Lambda_L}{\delta_f} \right)^{1/3} \quad (2)$$

It is observed that the data are mainly located in the corrugated flamelets and thin reaction zones regimes, Fig. 4.

2.3. Two-dimensional temperature measurement

The Rayleigh scattering technique was used to measure the two-dimensional temperature fields of premixed turbulent flames. The light source was a single-pulsed Nd:YAG laser (Spectra-Physics, Quanta-Ray, Lab-170-10) with a pulse energy and wavelength of 220 mJ and 355 nm, respectively. The laser beam was focused at the burner centerline using a UV-fused silica plano-concave lens, $f = -75$ mm, along with a plano-convex lens, $f = +100$ mm. The focused beam was then converted into a laser sheet of approximately 230 μm at full-width-at-half-maximum using a plano-concave cylindrical lens, $f = -25$ mm. An intensified CCD camera (NanoStar, LaVision) with a resolution of 1280×1024 px² was placed at a right angle to the laser sheet in order to collect the scattered light through a 355 nm bandpass filter. The intensifier was active over a 10 μs period in order to decrease the influence of flame radiation on the Rayleigh scattering images. The gain for the ICCD was equal to 60. The camera was equipped with a Sodern-Cerco UV lens with a focal length of 94 mm operating at $f/4.1$. The field-of-view imaged by the Rayleigh scattering system was approximately 128×102 mm² with a resolution of 100 $\mu\text{m}/\text{px}$. The DaVis 7.0 software (Rayleigh Thermometry, LaVision) was used to record five hundred Rayleigh scattering images at a frequency of 5 Hz for each flame condition. The noise on each of the

raw Rayleigh scattering image was reduced by employing a 3×3 pixel non-linear sliding average filter. The temperature field, $T_f(r, h)$, was then estimated using the following formula [27]:

$$T_f(r, h) = \frac{\sigma_m}{\sigma_a} T_a \frac{I_a - I_b}{I_R - I_b} = k T_a I, \quad (3)$$

where σ_m and σ_a are the fuel–air mixture and pure-air Rayleigh scattering cross sections, respectively. These parameters were evaluated from $\sigma_m = \left(\sum_i \sigma_i \chi_i \right)_m$ and $\sigma_a = \left(\sum_i \sigma_i \chi_i \right)_a$. The Rayleigh scattering cross section, σ_i , of the i th species was acquired from the results provided in [28]. The Cantera package [20] was used to estimate the mole fraction of each species, χ_i , by solving an adiabatic unstrained premixed laminar flame. T_a is the air temperature. I_R , I_a , and I_b are the intensity of the flame, reference, and background images, respectively. The reference image was captured under the non-reacting condition when the co-flow was utilized to eliminate dust particles from the flow field. The background intensity was evaluated by solving Eq. (3) in the burned region and setting $T_f = T_{ad}$, where T_{ad} is the adiabatic flame temperature [29]. For each image, the intensity ratio, I , demonstrated a bimodal distribution. The peaks of the intensity ratio were associated with the unburned and burned temperatures [30]. Furthermore, a correlation between the intensity ratio, I , and the ratio of the fuel–air mixture to the pure-air Rayleigh scattering cross sections, k , was established using a 4th order polynomial by relating the peaks of the intensity ratio to $k(T_u)$ and $k(T_{ad})$, where T_u is the unburned temperature. Therefore, the R.H.S of Eq. (3) was reduced to a single parameter of I at a fixed T_a . Further details of this procedure are explained in [30]. An instantaneous temperature field for a representative flame condition, Flame D3, is shown in Fig. 5.

3. Results and discussion

3.1. Flame brush characteristics

The mean progress variable, $\langle c \rangle$, was obtained by averaging over five hundred instantaneous progress variable fields. The instantaneous progress variable was defined from $c = (T_f - T_u)/(T_b - T_u)$, where T_b is the burned temperature. A contour plot of the mean progress variable for a representative flame condition, Flame C3, is shown in Fig. 6. The distance from the centerline of the burner exit to the half-burning surface, $\langle c \rangle = 0.5$, was considered as a

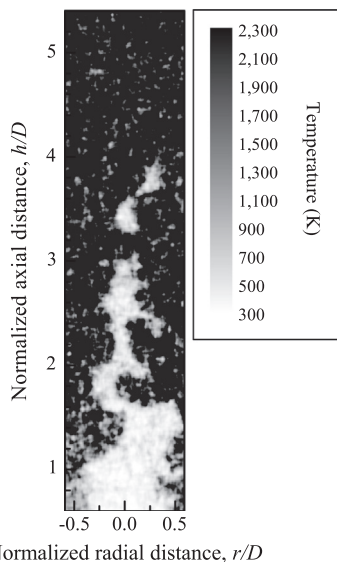


Fig. 5. Instantaneous temperature field for Flame D3.

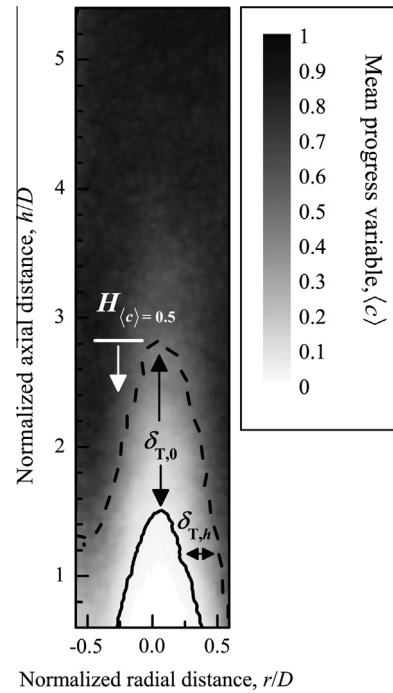


Fig. 6. Contour plot of the mean progress variable for Flame C3 along with the definitions of characteristic flame height, that is, $H_{\langle c \rangle = 0.5}$, and flame brush thicknesses, that is, $\delta_{T,0}$ and $\delta_{T,h}$. Solid and dash lines indicate the locations of $\langle c \rangle = 0.05$ and 0.5 , respectively.

characteristic flame height, $H_{\langle c \rangle = 0.5}$. For each set of experiments, the normalized characteristic flame height, $H_{\langle c \rangle = 0.5}/D$, decreased by increasing the equivalence ratio from 0.7 to 1.0, Fig. 7. Similar observations were previously reported in [6,7,9]. This trend could be attributed to the increase in flame temperature resulting in augmentation of the global reaction rate. The normalized characteristic flame height decreased by about 40% with a 3.5-fold increase in total turbulence intensity under a constant equivalence ratio (Flames A1–D1 and A2–D2 in Fig. 7), indicating that the global reaction rate increases due to an increase in the total turbulence intensity. Furthermore, by increasing the bulk flow velocity from 7.7 to 17.0 m/s (Flames A3–D3 and A4–D4 in Fig. 7), $H_{\langle c \rangle = 0.5}/D$ increased by a factor of 2.4 at a fixed equivalence ratio. Moreover, increasing the longitudinal integral length scale by a factor of approximately

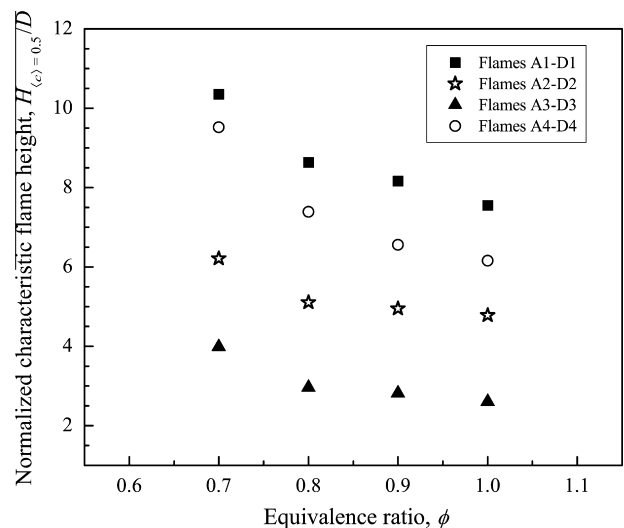


Fig. 7. Normalized characteristic flame height as a function of the equivalence ratio for all sets of experiments.

1.5 (Flames A1–D1 and A4–D4 in Fig. 7) results in a decrease in $H_{(c)=0.5}/D$ by approximately 8–20%. The characteristic flame height for all experimental conditions is summarized in Table 3.

The distance between the leading edge of the flame front, $(c) = 0.05$, and the half-burning surface, $(c) = 0.5$, was characterized as the flame brush thickness in this study. This definition was previously used in [9,31]. It is worth mentioning that the quantitative value of flame brush thickness varies significantly using different definitions, whereas the qualitative trend remains unaltered [32]. The definitions of centerline flame brush thickness, $\delta_{T,0}$, and horizontal flame brush thickness, $\delta_{T,h}$, are shown in Fig. 6. The normalized centerline flame brush thickness, $\delta_{T,0}/D$, changed linearly with the normalized characteristic flame height, $H_{(c)=0.5}/D$, and it decreased with increasing equivalence ratio for each set of experiments, Fig. 8. Experimental measurements of Griebel et al. [9] displayed a similar trend. The observed trend suggests that reactants are consumed within a smaller flame brush as a result of an increase in the global reaction rate with increasing equivalence ratios from 0.7 to 1.0. It should be noted that the centerline flame brush thickness decreases faster with increasing equivalence ratio for the third set of experiments in comparison with other sets of experiments. This implies that the lower bulk flow velocity in the third set of experiments might be the cause of this behavior. The centerline flame brush thickness for all sets of experiments is listed in Table 3.

The mean progress variable profiles at different axial distances from the burner exit mimicked the behavior of a complementary error function when the local distance across the flame brush, $\xi(h)$, was normalized by the local horizontal flame brush thickness, $\delta_{T,h}$, for the third set of experiments as a representative set, Fig. 9. It is worth mentioning that the coefficient in the error function approximation increased with increasing axial distance from the burner exit. The local distance across the flame brush was determined using the following expression:

$$\xi(h) = r(h) - r(h)_{(c)=0.5}, \quad (4)$$

where $r(h)$ is the radial distance from the centerline of the burner at a certain axial distance from the burner exit, h . Similar observations were previously reported for a Bunsen-type [7], V-shaped [33], and counterflow flames [34]. This observation suggests the existence of a universal characteristic for premixed turbulent flames which seems to be independent of the flame geometry [2].

The normalized horizontal flame brush thickness, $\delta_{T,h}/D$, obtained from the measured data increased with increasing normalized axial distance from the burner exit, h/D , for Flames

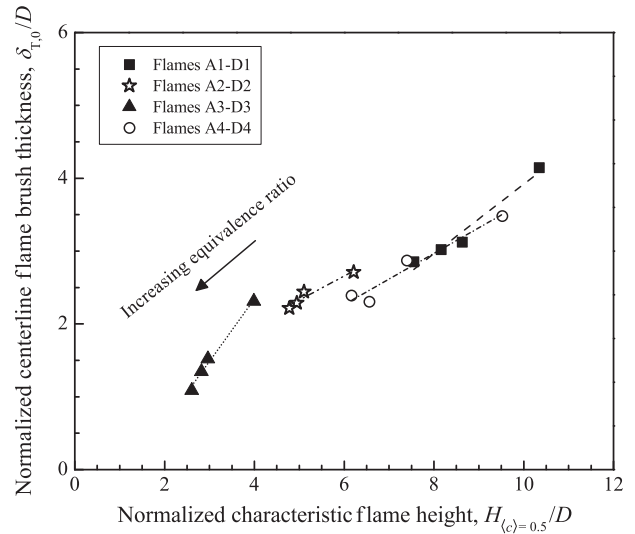


Fig. 8. Variation of the normalized centerline flame brush thickness with respect to the normalized characteristic flame height for all sets of experiments. The lines are least squares fits to the data.

D1–D4 as shown in Fig. 10. This development was supported by the Taylor hypothesis of turbulent diffusion [2]. The normalized horizontal flame brush thickness increased at a fixed h/D by increasing the total turbulence intensity (Flames D1 and D2 in Fig. 10), indicating that increasing the total turbulence intensity results in enlarging the zone occupied by the wrinkled flamelets. Experimental findings of Venkateswaran [32] showed a similar trend for H_2/CO mixtures. Furthermore, increasing the bulk flow velocity resulted in a decrease in $\delta_{T,h}/D$ at a constant h/D (Flames D3 and D4 in Fig. 10), suggesting that the flame front wrinkling decreases with increasing bulk flow velocity. Moreover, increasing the longitudinal integral length scale led to a slight increase in $\delta_{T,h}/D$ (Flames D1 and D4 in Fig. 10). This observation suggests that the zone occupied by the wrinkled flamelets increases with increasing longitudinal integral length scale.

The horizontal flame brush thickness normalized by the burner diameter, $\delta_{T,h}/D$, as a function of the normalized axial distance from the burner exit, h/D , for all experimental conditions is shown in Fig. 11. Results show that the horizontal flame brush thickness increased with increasing equivalence ratios from 0.7 to 1.0. Similar observations were reported previously in [7,33].

Table 3

Summary of experimental results. Symbols: ϕ = equivalence ratio; U_B = bulk flow velocity; u' = total turbulence intensity; S_L^0 = unstrained premixed laminar burning velocity; Λ_L = longitudinal integral length scale; δ_f = Zel'dovich thickness; $H_{(c)=0.5}$ = characteristic flame height; $\delta_{T,0}$ = centerline flame brush thickness; $S_{T,(c)=0.05}$ = leading edge turbulent burning velocity; $S_{T,(c)=0.5}$ = half-burning surface turbulent burning velocity.

Set of exp.	Flame	ϕ	U_B/S_L^0	u'/S_L^0	Λ_L/δ_f	$H_{(c)=0.5}$ (mm)	$\delta_{T,0}$ (mm)	$S_{T,(c)=0.05}$ (m/s)	$S_{T,(c)=0.5}$ (m/s)	$S_{T,(c)=0.05}/S_{T,(c)=0.5}$
I	A1	0.7	85.6	3.5	13.5	115.1	46.1	1.35	0.43	3.13
	B1	0.8	60.9	2.5	19.0	96.0	34.7	1.41	0.56	2.52
	C1	0.9	49.3	2.0	23.5	90.8	33.6	1.33	0.54	2.44
	D1	1.0	44.0	1.8	26.4	84.0	31.7	1.66	0.67	2.47
II	A2	0.7	85.6	12.3	12.8	69.1	30.2	2.46	0.77	3.17
	B2	0.8	60.9	8.7	18.1	56.8	27.2	3.13	0.87	2.47
	C2	0.9	49.3	7.1	22.4	55.0	25.4	2.96	0.85	3.47
	D2	1.0	44.0	6.3	25.2	53.2	24.7	2.94	0.81	3.63
III	A3	0.7	38.9	3.7	19.9	44.3	25.7	1.99	0.68	2.92
	B3	0.8	27.6	2.6	28.1	33.0	16.9	2.32	0.93	2.49
	C3	0.9	22.3	2.1	34.8	31.3	15.0	2.16	0.91	2.37
	D3	1.0	19.9	1.9	39.1	29.0	12.1	2.26	0.97	2.33
IV	A4	0.7	85.6	3.7	21.0	105.9	38.7	1.34	0.57	2.35
	B4	0.8	60.9	2.7	28.5	82.3	31.9	1.52	0.72	2.11
	C4	0.9	49.3	2.2	34.1	73.0	25.6	0.80	0.80	2.00
	D4	1.0	44.0	2.0	40.2	68.5	26.6	1.94	0.88	2.21

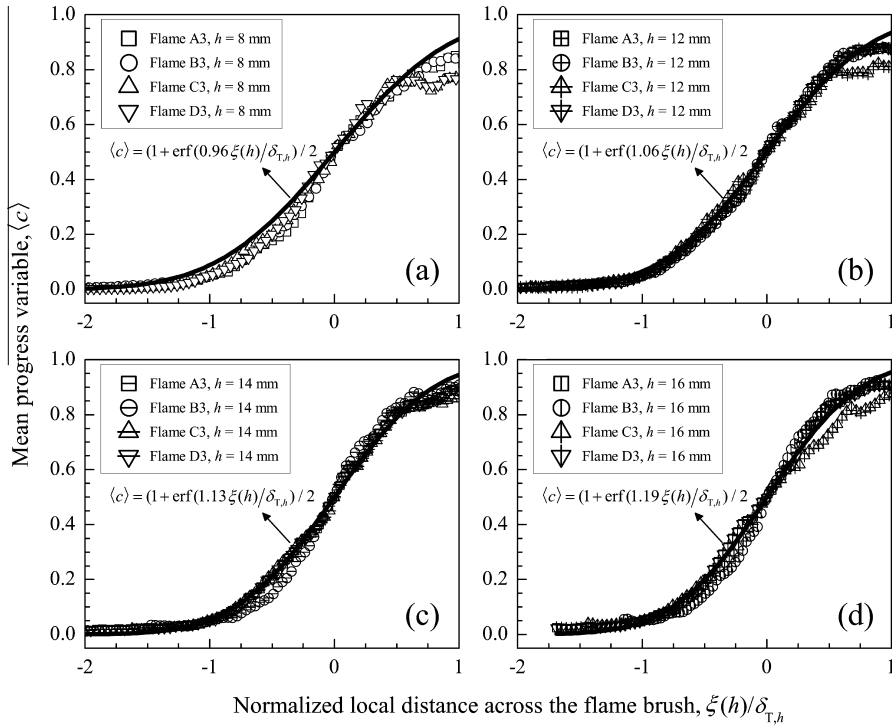


Fig. 9. Mean progress variable profiles as a function of the normalized local distance across the flame brush for the third set of experiments at (a) $h = 8$ mm, (b) $h = 12$ mm, (c) $h = 14$ mm, and (d) $h = 16$ mm.

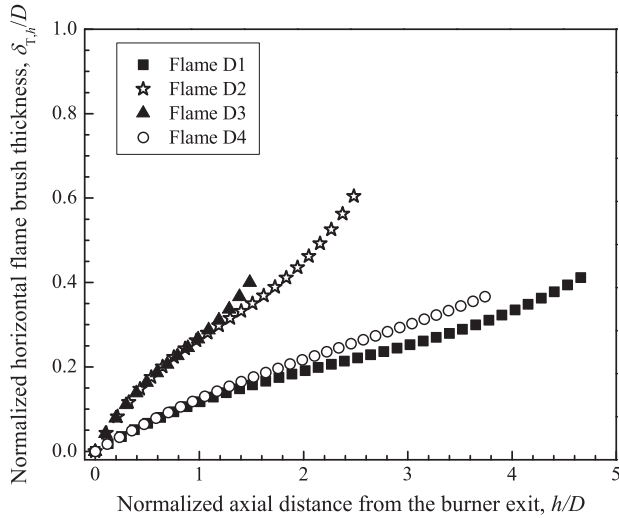


Fig. 10. Variation of the normalized horizontal flame brush thickness with respect to the normalized axial distance from the burner exit for Flames D1–D4.

3.2. Turbulent burning velocity

The turbulent burning velocity, $S_{T,(c)}$, conditioned at a specific mean progress variable, $\langle c \rangle$, was estimated using the following expression:

$$S_{T,(c)} = U_B \frac{A_0}{A_{T,(c)}}, \quad (5)$$

where A_0 is the cross-sectional area of the burner exit, and $A_{T,(c)}$ is the turbulent mean flame front surface area conditioned at $\langle c \rangle$. The mean flame front surface was created by rotating the mean flame front around the h -axis in a virtual environment. The leading edge and half-burning surface turbulent burning velocities were determined by conditioning the mean progress variables at 0.05 and

0.5, respectively. The half-burning surface turbulent burning velocity can be a representative of the overall consumption velocity. The systematic error in estimation of $S_{T,(c)}$, originating from the uncertainties in air and fuel flow measurements, and in calculation of $A_{T,(c)}$, is about 1.5%. The non-dimensional leading edge and half-burning surface turbulent burning velocities with respect to the non-dimensional turbulence intensity, u'/S_L^0 , for the first and second sets of experiments are presented in Fig. 12(a) and Fig. 12(b), respectively. The leading edge turbulent burning velocity, $S_{T,(c)=0.05}$, was higher than the half-burning surface turbulent burning velocity, $S_{T,(c)=0.5}$, for each flame condition due to an increase in $A_{T,(c)}$ with increasing mean progress variable, see Eq. (5). Results show that the non-dimensional leading edge and half-burning surface turbulent burning velocities increased with increasing non-dimensional turbulence intensity. Similar trends were previously reported for a Bunsen-type burner, see, e.g., [8,9,35,36]. In addition, increasing the total turbulence intensity from 0.69 to 2.44 m/s led to an increase in $S_{T,(c)=0.05}/S_L^0$ by a factor of 1.8–2.2, and in $S_{T,(c)=0.5}/S_L^0$ by a factor of 1.2–1.8. The primary reason behind this trend could be the increase in the local flame surface area with turbulent structures [37].

The non-dimensional turbulence intensity was increased by a factor of 3.5 from the first to the second set of experiments under a constant equivalence ratio, whereas the non-dimensional bulk flow velocity, U_B/S_L^0 , and non-dimensional longitudinal integral length scale, Λ_L/δ_f , were kept constant, see Table 2. For the first and second sets of experiments, Ξ_1 and Υ_1 are defined as follows:

$$\Xi_1 = \frac{(S_{T,(c)} - S_L^0)_{I,\phi}}{(S_{T,(c)} - S_L^0)_{II,\phi}} = \frac{(u')_I^{\alpha_1}}{(u')_{II}^{\alpha_1}} = \Upsilon_1^{\alpha_1}. \quad (6)$$

The values of Ξ_1 were found to be independent from the equivalence ratio. The value of α_1 was then estimated to be approximately 0.62 for both the leading edge and half-burning surface. Therefore, $(S_{T,(c)} - S_L^0)/S_L^0$ increased linearly with respect to $(u'/S_L^0)^{0.62}$ for these flame conditions, Fig. 13.

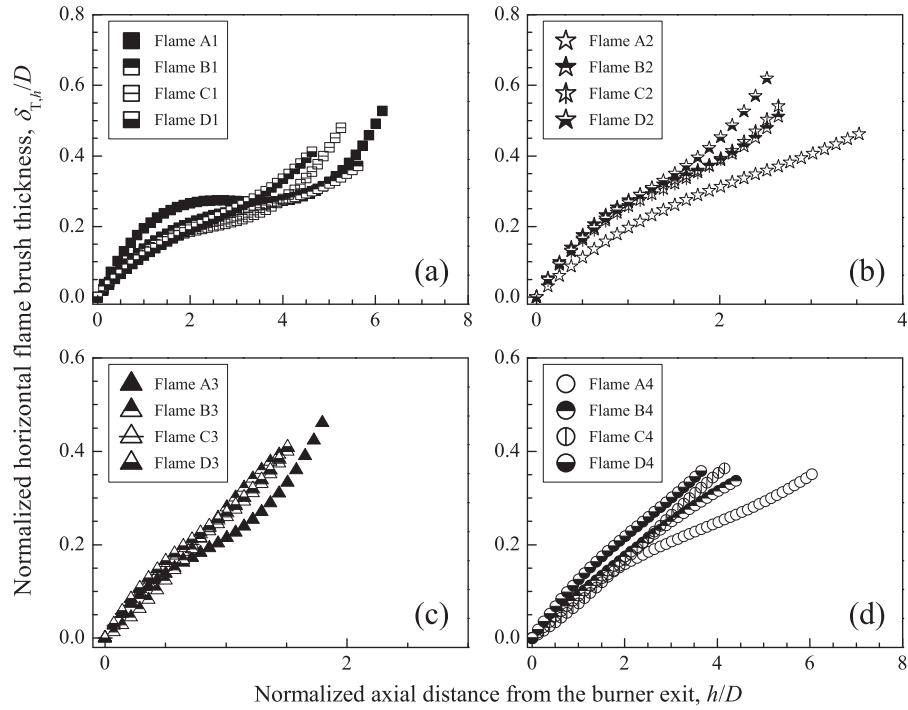


Fig. 11. Normalized horizontal flame brush thickness as a function of the normalized axial distance from the burner exit for the (a) first set of experiments, (b) second set of experiments, (c) third set of experiments, and (d) fourth set of experiments.

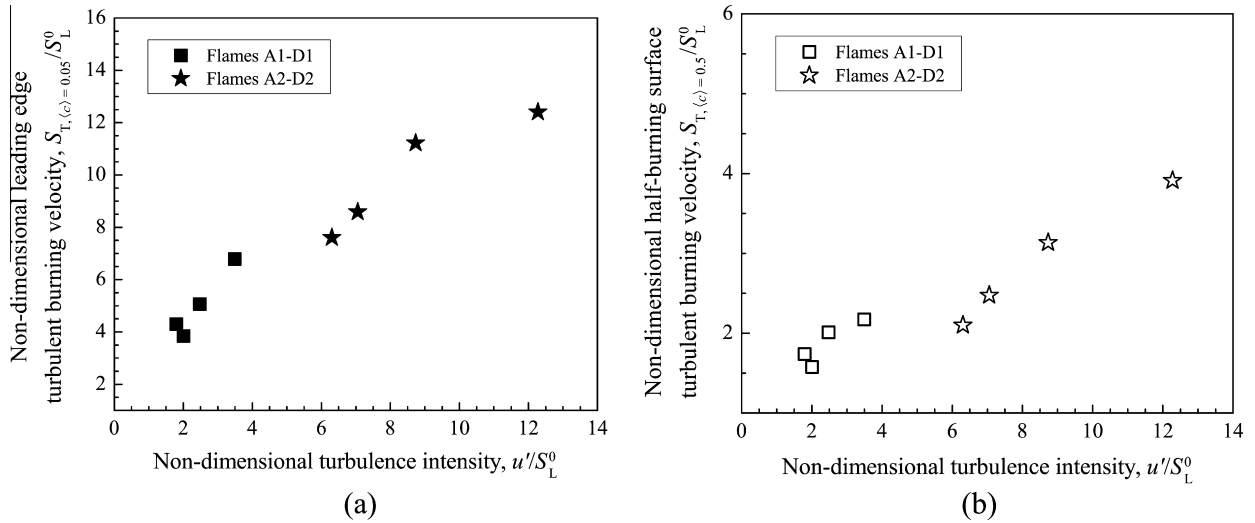


Fig. 12. (a) Non-dimensional leading edge turbulent burning velocity and (b) non-dimensional half-burning surface turbulent burning velocity as a function of the non-dimensional turbulence intensity for the first and second sets of experiments. The lowest u/S_L^0 for each set of experiments corresponds to the flame condition at $\phi = 1.0$, and it increases with decreasing equivalence ratio.

The non-dimensional leading edge and half-burning surface turbulent burning velocities with respect to the non-dimensional turbulence intensity for the third and fourth sets of experiments are shown in Fig. 14(a) and Fig. 14(b), respectively. It is observed that increasing the bulk flow velocity from 7.7 to 17.0 m/s under a constant non-dimensional turbulence intensity results in the leading edge and half-burning surface turbulent burning velocities to decrease. The observed trend might be attributed to the formation of local extinctions which are created due to the increase of flame front stretching caused by the existence of large velocity gradients in shear layers [9]. This trend is in contrast with the turbulent burning velocity correlation for a slot Bunsen burner proposed

in [4], in which the turbulent burning velocity was shown to increase with the bulk flow velocity.

The non-dimensional bulk flow velocity, U_B/S_L^0 , increased by a factor of 2.2 under a constant equivalence ratio from the third to the fourth set of experiments, whereas the non-dimensional turbulence intensity and longitudinal integral length scale were kept constant, see Table 2. For the third and fourth sets of experiments, Ξ_2 and Υ_2 are defined as follows:

$$\Xi_2 = \frac{(S_{T,(c)} - S_L^0)_{III,\phi}}{(S_{T,(c)} - S_L^0)_{IV,\phi}} = \frac{(U_B)_{III}^{z_2}}{(U_B)_{IV}^{z_2}} = \Upsilon_2^{z_2}. \quad (7)$$

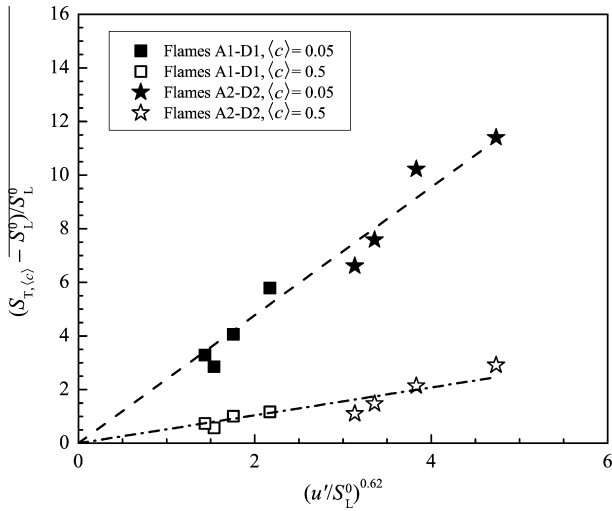
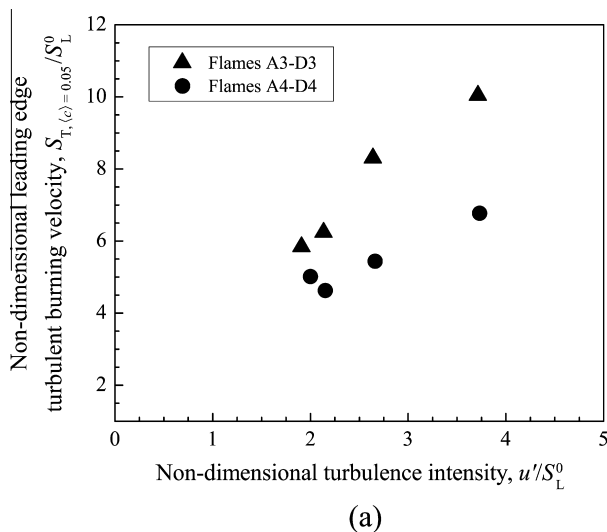


Fig. 13. Variation of $(S_{T,(c)} - S_L^0)/S_L^0$ with respect to $(u'/S_L^0)^{0.62}$ for the first and second sets of experiments. Dash and dash-dot lines are least squares fits with the slopes of approximately 2.4 and 0.5, respectively.

The value of α_2 was evaluated to be approximately -0.52 and -0.36 for the leading edge and half-burning surface, respectively. For these sets of experiments, $(S_{T,(c)} - S_L^0)/S_L^0$ increased linearly with respect to $(u'/S_L^0)^{0.62} (U_B/S_L^0)^{-0.52}$ for the leading edge, and $(u'/S_L^0)^{0.62} (U_B/S_L^0)^{-0.36}$ for the half-burning surface as shown in Fig. 15(a) and Fig. 15(b), respectively.

The leading edge and half-burning surface turbulent burning velocities for the fourth set of experiments were higher than the corresponding values for the first set of experiments at a constant non-dimensional turbulence intensity (compare Figs. 12 and 14). This discrepancy could be attributed to the differences in the non-dimensional longitudinal integral length scale under a constant equivalence ratio, whereas the non-dimensional turbulence intensity and bulk flow velocity were kept constant. Therefore, the scaling between the first and fourth sets of experiments is defined as follows:



$$\Xi_3 = \frac{(S_{T,(c)} - S_L^0)_{I,\phi}}{(S_{T,(c)} - S_L^0)_{IV,\phi}} = \frac{(\Lambda_L)_I^{\alpha_3}}{(\Lambda_L)_{IV}^{\alpha_3}} = \Upsilon_3^{\alpha_3} \quad (8)$$

The value of α_3 was evaluated to be approximately 0.2 and 1.35 for the leading edge and half-burning surface, respectively. It is worth mentioning that the longitudinal integral length scale in the reactant region was used as a reference value for evaluation of α_3 . This may explain the large difference occurs in the value of α_3 for the leading edge and half-burning surface due to the fact that the integral length scales near the leading edge of the flame are strongly affected by the turbulence produced at the inlet of the burner, whereas these scales could change near the half-burning surface because of the existence of shear layers. The exponential proportionality of turbulent burning velocity to integral length scale has been previously observed, see, e.g., [38]. However, Andrews et al. [38] reported that the value of the exponent is equal to 0.5. The non-dimensional longitudinal integral length scale, Λ_L/δ_f , along with previous parameters investigated in this study, that is, ϕ , u'/S_L^0 , and U_B/S_L^0 , could be then incorporated in the development of a general correlation for the turbulent burning velocity of Bunsen flames. Therefore, two correlations to represent the leading edge and half-burning surface turbulent burning velocities are developed as follows:

$$\frac{S_{T,(c)=0.05}}{S_L^0} = 1 + A_1 \left(\frac{u'}{S_L^0}\right)^{0.62} \left(\frac{U_B}{S_L^0}\right)^{-0.52} \left(\frac{\Lambda_L}{\delta_f}\right)^{0.2} \quad (9a)$$

$$\frac{S_{T,(c)=0.5}}{S_L^0} = 1 + A_2 \left(\frac{u'}{S_L^0}\right)^{0.62} \left(\frac{U_B}{S_L^0}\right)^{-0.36} \left(\frac{\Lambda_L}{\delta_f}\right)^{1.35} \quad (9b)$$

The non-dimensional turbulent burning velocity, $S_{T,(c)}/S_L^0$, increased linearly with respect to the variables presented on the R.H.S of Eq. (9a) for the leading edge, and Eq. (9b) for the half-burning surface as shown in Fig. 16(a) and Fig. 16(b), respectively. It is worth noting that A_1 and A_2 can be expressed as a function of the equivalence ratio as $A_1 = 7.60\phi^{-1.87}$ and $A_2 = 0.018\phi^{-4.03}$. This dependency could be due to thermo-diffusive effects, but the global Lewis number, which is about unity for these mixtures, would not support this dependency. The summary of the leading edge and half-burning surface turbulent burning velocities for all sets of experiments is

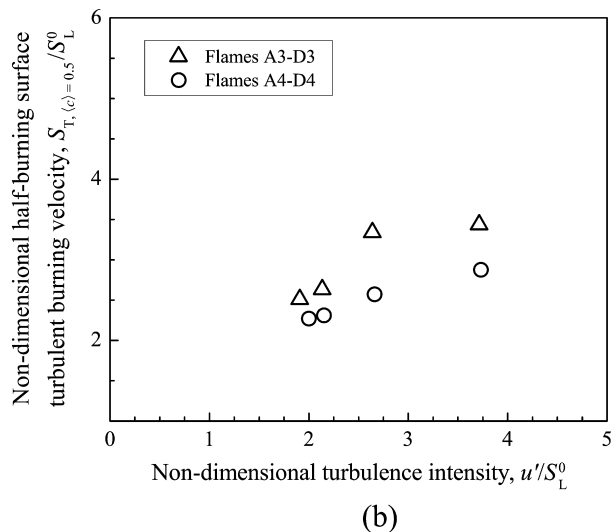


Fig. 14. (a) Non-dimensional leading edge turbulent burning velocity and (b) non-dimensional half-burning surface turbulent burning velocity as a function of the non-dimensional turbulence intensity for the third and fourth sets of experiments. For each set of experiments, u'/S_L^0 increases with decreasing equivalence ratios from 1.0 to 0.7.

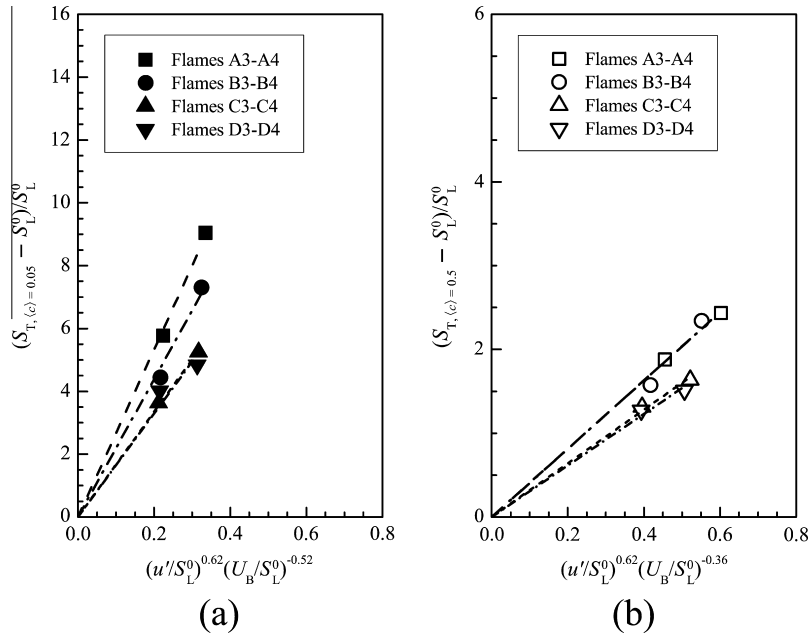


Fig. 15. Variation of $(S_{T,(c)} - S_L^0)/S_L^0$ with respect to (a) $(u'/S_L^0)^{0.62} (U_B/S_L^0)^{-0.52}$ for the leading edge and (b) $(u'/S_L^0)^{0.62} (U_B/S_L^0)^{-0.36}$ for the half-burning surface for the third and fourth sets of experiments. The lines indicate least squares fits to the data. The slopes of these lines are dependent on the equivalence ratio, and they decreased with increasing equivalence ratios from 0.7 to 1.0.

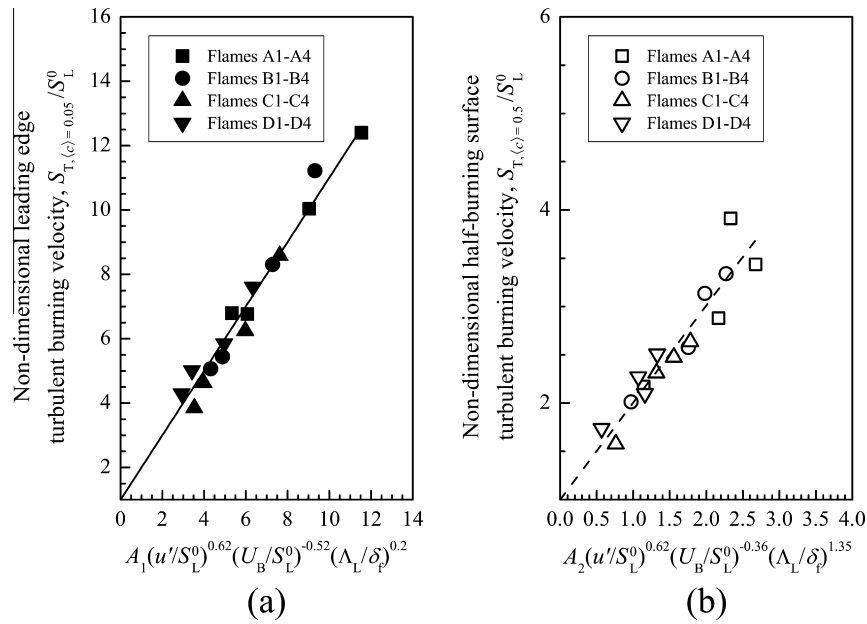


Fig. 16. Non-dimensional turbulent burning velocity, $S_{T,(c)}/S_L^0$, for all flame conditions with respect to the variables presented on the R.H.S of (a) Eq. (9a) for the leading edge and (b) Eq. (9b) for the half-burning surface. Solid and dash lines indicate least squares fits to the measured data.

tabulated in Table 3. Results show that the leading edge and half-burning surface turbulent burning velocities increased with increasing equivalence ratios from 0.7 to 1.0 for the first and fourth sets of experiments at $u'/U_B \approx 4.0\%$. However, these velocities were invariant with increasing equivalence ratios from 0.8 to 1.0 for the second and third sets of experiments at $u'/U_B = 14.4\%$ and 9.5% , respectively. The data presented in [8] showed a similar behavior with increasing u'/U_B from 10% to 18%. The ratio of the leading edge to the half-burning surface turbulent burning velocity, $S_{T,(c)=0.05}/S_{T,(c)=0.5}$, varies from 2.0 to 3.6, see Table 3, whereas Smallwood et al. [39] proposed that this ratio changes from 1.2 to 1.5 for

Bunsen flames. This discrepancy may be due to the different methods used to determine the mean flame surface area and different ranges of non-dimensional turbulence intensity tested.

The half-burning surface turbulent burning velocity normalized by the bulk flow velocity, $S_{T,(c)=0.5}/U_B$, decreased with increasing normalized characteristic flame height, $H_{(c)=0.5}/D$, as shown in Fig. 17. The data from [8] are also shown in Fig. 17. It should be stated that the inner diameter of the burner for the aforementioned experiments is 2.7 times larger than the burner of the current study. A least squares fit to each data set shown in Fig. 17 gives the following expression:

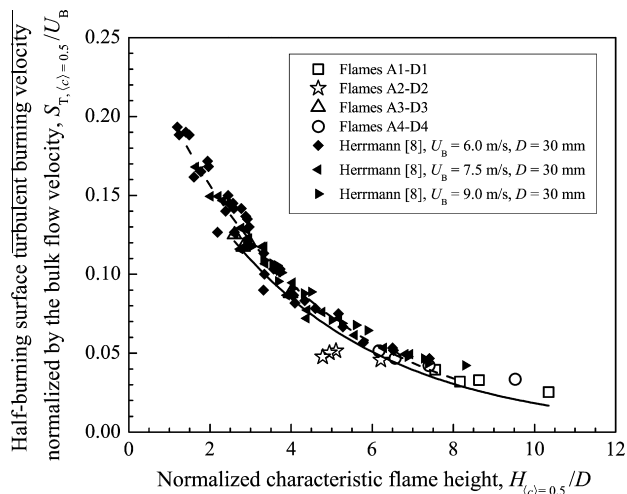


Fig. 17. Variation of the half-burning surface turbulent burning velocity normalized by the bulk flow velocity, $S_{T,(c)=0.5}/U_B$, with respect to the normalized characteristic flame height, $H_{(c)=0.5}/D$. Solid and dash lines are least squares fits to the experimental conditions of the current work and previous study [8], respectively.

$$\frac{S_{T,(c)=0.5}}{U_B} = B_1(B_2)^{H_{(c)=0.5}/D}, \quad (10)$$

where B_1 is equal to approximately 0.23 and 0.26 for the current work and previous study [8], respectively, and B_2 is equal to approximately 0.77 for both studies. This correlation seems to predict the half-burning surface turbulent burning velocity of premixed turbulent methane/air Bunsen flames by knowing the bulk flow velocity, U_B , and characteristics flame height, $H_{(c)=0.5}$. It is worth noting that the universal behavior of Eq. (10) for premixed turbulent Bunsen flames should be checked by performing further experiments with different mixture compositions.

4. Concluding remarks

The flame brush characteristics and turbulent burning velocities of premixed turbulent methane/air Bunsen-type flames were investigated in the current work. The instantaneous velocity and temperature fields of premixed turbulent flames were measured using the particle image velocimetry and Rayleigh scattering techniques, respectively. The total turbulence intensity and turbulent integral length scale were controlled by the perforated plate mounted at various locations upstream of the burner exit. This resulted in the non-dimensional turbulence intensity changing from 1.8 to 12.3. All experimental conditions are located in the corrugated flamelets and thin reaction zones regimes.

The normalized characteristic flame height decreased with increasing equivalence ratio, total turbulence intensity, and longitudinal integral length scale, whereas it increased with increasing bulk flow velocity.

The variation of the normalized centerline flame brush thickness was similar to the behavior of normalized characteristic flame height. The mean progress variable profiles at various axial distances from the burner exit were similar to the complementary error function when the local distance across the flame brush was normalized by the local horizontal flame brush thickness. The normalized horizontal flame brush thickness developed with increasing axial distance from the burner exit and increasing equivalence ratios from 0.7 to 1.0. The normalized horizontal flame brush thickness increased with increasing total turbulence intensity, whereas it decreased with increasing bulk flow velocity under

a constant equivalence ratio. It increased slightly by increasing the longitudinal integral length scale.

The non-dimensional leading edge and half-burning surface turbulent burning velocities increased with increasing non-dimensional turbulence intensity, and they decreased with increasing non-dimensional bulk flow velocity. The non-dimensional leading edge and half-burning surface turbulent burning velocities increased with increasing non-dimensional longitudinal integral length scale for the conditions tested in this study. Two correlations to represent the leading edge and half-burning surface turbulent burning velocities were derived with respect to the equivalence ratio, non-dimensional turbulence intensity, non-dimensional bulk flow velocity, and non-dimensional longitudinal integral length scale. Results show that the half-burning surface turbulent burning velocity normalized by the bulk flow velocity decreased with increasing normalized characteristic flame height.

Acknowledgment

The financial support from the Natural Sciences and Engineering Research Council of Canada (NSERC) is acknowledged.

Appendix A. Supplementary material

Supplementary data associated with this article can be found in the online version, at <http://dx.doi.org/10.1016/j.combustflame.2014.06.014>.

References

- [1] N. Peters, *Turbulent Combustion*, Cambridge University Press, Cambridge, 2000.
- [2] A.N. Lipatnikov, J. Chomiak, *Prog. Energy Combust. Sci.* 28 (2002) 1–74.
- [3] R.K. Cheng, I.G. Shepherd, *Combust. Flame* 85 (1991) 7–26.
- [4] S.A. Filatyev, J.F. Driscoll, C.D. Carter, J.M. Donbar, *Combust. Flame* 141 (2005) 1–21.
- [5] R. Bilger, S. Pope, K.N.C. Bray, J.F. Driscoll, *Proc. Combust. Inst.* 30 (2005) 21–42.
- [6] B. Deschamps, Étude spatiale et temporelle de la structure dynamique et scalaire des flammes turbulentes premelangees de méthane-air, Ph.D. thesis, University of Orléans, 1990.
- [7] A. Boukhalfa, I. Gökalp, *Combust. Flame* 73 (1988) 75–87.
- [8] K. Herrmann, Strömung, flammencharakterisierung und stickoxid-bildung in turbulenten vormischflammen, Ph.D. thesis, ETH Zürich, 2002.
- [9] P. Griebel, P. Siewert, P. Jansohn, *Proc. Combust. Inst.* 31 (2007) 3083–3090.
- [10] Ö.L. Gülder, *Proc. Combust. Inst.* 23 (1990) 743–750.
- [11] C.C. Liu, S.S. Shy, M.W. Peng, C.W. Chiu, Y.C. Dong, *Combust. Flame* 159 (2012) 2608–2619.
- [12] J.F. Driscoll, *Prog. Energy Combust. Sci.* 34 (2008) 91–134.
- [13] P. Siewert, Flame front characteristics of turbulent lean premixed methane/air flames at high-pressure, Ph.D. thesis, ETH Zürich, 2006.
- [14] Ö.L. Gülder, G.J. Smallwood, *Combust. Sci. Technol.* 179 (2007) 191–206.
- [15] F.T.C. Yuen, Ö.L. Gülder, *Proc. Combust. Inst.* 32 (2009) 1747–1754.
- [16] F.T.C. Yuen, Experimental investigation of the dynamics and structure of lean-premixed turbulent combustion, Ph.D. thesis, University of Toronto Institute for Aerospace Studies, 2009.
- [17] Y.C. Chen, R.W. Bilger, *Combust. Sci. Technol.* 167 (2001) 131–167.
- [18] Y.C. Chen, R.W. Bilger, *Exp. Therm. Fluid Sci.* 27 (2003) 619–627.
- [19] G.K. Batchelor, *The Theory of Homogeneous Turbulence*, Cambridge University Press, 1953.
- [20] D. Goodwin, N. Malaya, H.K. Moffat, R. Speth, Cantera. <<http://code.google.com/p/cantera/>>.
- [21] G.P. Smith, D.M. Golden, M. Frenklach, N.W. Moriarty, B. Eiteneer, M. Goldenberg, C.T. Bowman, R.K. Hanson, S. Song, W.C. Gardiner, V.V. Lissianski, Z. Qin, GRI-Mech 3.0. <http://www.me.berkeley.edu/gri_mech/>.
- [22] G. Yu, C.K. Law, C.K. Wu, *Combust. Flame* 63 (1986) 339–347.
- [23] A. Van Maaren, D.S. Thung, L.P.H. de Goey, *Combust. Sci. Technol.* 96 (1994) 327–344.
- [24] T. Boushaki, Y. Dhué, L. Selle, B. Ferret, T. Poinso, *Int. J. Hydrogen Energy* 37 (2012) 9412–9422.
- [25] R. Borghi, in: C. Casci, C. Bruno (Eds.), *Recent Advances in Aerospace Sciences*, Plenum Press, New York, 1985, pp. 117–138.
- [26] N. Peters, *J. Fluid Mech.* 384 (1999) 107–132.
- [27] A. Soika, F. Dinkelacker, A. Leipertz, *Proc. Combust. Inst.* 27 (1998) 785–792.
- [28] J.A. Sutton, J.F. Driscoll, *Opt. Lett.* 29 (2004) 2620–2622.
- [29] D.A. Knaus, S.S. Sattler, F.C. Gouldin, *Combust. Flame* 141 (2005) 253–270.
- [30] F.T.C. Yuen, Ö.L. Gülder, *AIAA J.* 47 (2009) 2964–2973.
- [31] V.P. Karpov, E.S. Severin, *Combust. Explos. Shock Waves* 14 (1978) 158–163.

- [32] P. Venkateswaran, Measurements and modeling of turbulent consumption speeds of syngas fuel blends, Ph.D. thesis, Georgia Institute of Technology, 2013.
- [33] M. Namazian, I.G. Shepherd, L. Talbot, *Combust. Flame* 64 (1986) 299–308.
- [34] C. Mounaïm-Rousselle, I. Gökalp, *Proc. Combust. Inst.* 25 (1994) 1199–1205.
- [35] P. Venkateswaran, A. Marshall, D.H. Shin, D. Noble, J. Seitzman, T. Lieuwen, *Combust. Flame* 158 (2011) 1602–1614.
- [36] F.T.C. Yuen, Ö.L. Gülder, *Proc. Combust. Inst.* 34 (2013) 1393–1400.
- [37] G. Damköhler, *Z. Electrochem.* 46 (1940) 601–652.
- [38] G.E. Andrews, D. Bradley, S.B. Lwakabamba, *Combust. Flame* 24 (1975) 285–304.
- [39] G.J. Smallwood, Ö.L. Gülder, D.R. Snelling, B.M. Deschamps, I. Gökalp, *Combust. Flame* 101 (1995) 461–470.